Combining single-particle inductively coupled plasma mass spectrometry and X-ray absorption spectroscopy to evaluate the release of colloidal arsenic from environmental samples

Miguel Angel Gomez-Gonzalez [1], Eduardo Bolea [2], Peggy A. O'Day [3], Javier Garcia-Guinea [1], Fernando Garrido [1], Francisco Laborda [2 *]

[1] *National Museum of Natural Sciences, CSIC, Jose Gutierrez Abascal 2, 28006 Madrid, Spain.*

[2] *Group of Analytical Spectroscopy and Sensors (GEAS), Institute of Environmental Sciences (IUCA), University of Zaragoza, Pedro Cerbuna 12, 50009 Zaragoza, Spain.*

[3] *Environmental Systems Program, University of California, Merced, CA 95343, USA.*

[*] corresponding author (e-mail: flaborda@unizar.es).

Keywords: Single particle, SP-ICP-MS, XAS, arsenic, colloids, scorodite

ABSTRACT

Detection and sizing of natural colloids involved in the release and transport of toxic metals and metaloids is essential to understand and model their environmental effects. Single-particle inductively coupled plasma mass spectrometry (SP-ICP-MS) was applied for the detection of arsenic-bearing particles released from mine wastes. Arsenic-bearing particles were detected in leachates from mine wastes, with a mass-per-particle detection limit of 0.64 ng of arsenic. Conversion of the mass-per-particle information provided by SP-ICP-MS into size information requires knowledge of the nature of the particles; therefore, synchrotron-based X-ray absorption spectroscopy (XAS) was used to identify scorodite ($FeAsO_4.2H_2O$) as the main species in the colloidal particles isolated by ultrafiltration. The size of the scorodite particles detected in the leachates was below 300-350 nm, in good agreement with the values obtained by TEM. The size of the particles detected by SP-ICP-MS was determined as the average edge of scorodite crystals, which show a rhombic dipiramidal form, achieving a size detection limit of 117 nm. The combined use of SP-ICP-MS and XAS allowed detection, identification and size determination of scorodite particles released from mine wastes, suggesting their potential to transport arsenic.

INTRODUCTION

Natural colloids, having sizes between 1 nm and 1 μm, are known to play a significant role as environmental vectors of toxic elements in relation with the contamination of soil-water systems [1]. Although the study of the processes involved in transport of colloids and its relevance to global element cycling is an active research field [2], current understanding of metal(loid) colloid mobilization and transport is still limited, in part by a lack of reliable analytical methods. The development of new analytical methods to isolate, identify and characterize micro- and nano-particles acting as metal(loid) carriers is needed to determine the chemical speciation and mode of dispersion in the environment of these toxic pollutants.

The mobility of arsenic in environmental systems is controlled by sorption, precipitation and dissolution processes that are tied directly to coupled reactions with iron and sulfur species [3], so that the speciation of As ultimately controls its release and transport in a variety of environmental scenarios, such as tailings at abandoned mines [4]. Scorodite ($FeAsO_4.2H_2O$) is the least soluble arsenate phase present in mine tailing systems, being also used by metallurgical industries to minimize As release into the environment [5]. The low solubility of scorodite limits the spread of As in acid mine-drainage at mine sites, and thus the formation of scorodite is a desired secondary weathering phase of arsenopyrite or As-bearing pyrite [6]. However, there is concern that scorodite would not be stable over the long term and would convert to ferric oxyhydroxide, with the concomitant release of As to the soil solution [7,8].

Conventional methods for the characterization of colloids based on size and composition relies mostly on transmission electron microscopy [4,9] and light scattering techniques [10]. In addition, conventional (ultra)filtration in combination with atomic spectrometry has been applied [11]. More recently, the emergence of flow field-flow

fractionation (FFFF) techniques coupled to different detectors has allowed the detailed characterization of natural colloids [12,13]. This separation technique has allowed study of metal(loid) species associated with microparticles, colloids and macromolecules in aqueous samples, within the size range of 1 kDa to 50 μm [14]. Nevertheless, the nature of the colloidal samples (e.g., high acidity and/or high ionic strength) can prevent the use of flow field-flow fractionation, due to the irreversible retention of the coloidal particle into the separation channel [15].

More recently, single-particle inductively coupled plasma mass spectrometry (SP-ICP-MS) has emerged as a feasible methodology for the analysis of micro and nanoparticles, providing information about size distributions and particle number concentrations, at levels down to thousands of particles per mL (ng L^{-1} expressed as mass concentration) [16,17]. In SP-ICP-MS, sufficiently diluted particle suspensions and high data acquisition frequencies are required to ensure that just one particle is measured during each reading period. Once entering into the ICP, the particles are vaporized, atomized and ionized, producing a cloud of gaseous ions in the plasma, which can be measured as a single pulse. Under such conditions, the frequency of the pulses is proportional to the number concentration of particles, and the number of counts of each pulse is related to the number of atoms of the monitored element in the particle, and hence to the mass of element per particle, which, in turn, can provide information about the size of the particle [18]. As a first approximation, SP-ICP-MS allows the detection of elements in particulate forms or associated to particles. However, additional information about the nature of the particles analyzed is needed (composition, shape and density) to convert the mass of element per particle provided by SP-ICP-MS into particle size. When this information is not available, assumptions

have to be made, as for Zn-bearing particles detected in surface and waste waters, whose sizes were estimated under the assumption of spherical ZnO particles [19].

The feasibility of SP-ICP-MS was demonstrated by Degueldre et al. [20], who applied this methodology to the analysis of synthetic colloidal and microparticle suspensions [21,22]. Currently, there is an increasing interest in the use of SP-ICP-MS for the detection, determination, and characterization of pristine engineered nanomaterials, and also of these nanomaterials in environmental and biological samples. However, its application in the field of environmental colloids is practically non-existent, and to the best of our knowledge, this is the first time that SP-ICP-MS has been applied to detect and characterize the size of As-bearing colloids. The aim of this work is to evaluate SP-ICP-MS as a potential technique for the detection of colloidal As mobilized from mine wastes, and to use X-ray absorption spectroscopy in combination to identify the nature of the colloidal particles and to estimate their size.

MATERIALS AND METHODS

Standards and chemicals

Diluted suspensions of gold nanoparticles were prepared from reference material RM 8013 (National Institute of Standards and Technology, NIST, USA) with a nominal diameter of 60 nm. Arsenic solutions were prepared from a standard stock solution of 100 mg L^{-1} (*Trace Metal Standard I*, J.T.Baker, Philipsburg, USA) by dilution in ultrapure water.

A synthetic scorodite ($Fe^{III}As^{V}O_4 \cdot 2H_2O$) was prepared following the procedure described by Voegelin et al. [23] and adapted from Hsu and Sikora [24]. Thirty milliliters of 0.5 M KH_2AsO_4 (Merck, Darmstadt, Germany) were mixed with 50 mL of 1 M HCl and 100 mL ultrapure water. Subsequently, 20 mL of 0.5 M $FeCl_3 \cdot 6H_2O$

(Merck, Darmstadt, Germany) were rapidly added. The precipitate was aged for 9 days at 90 ºC and then washed twice and dried. The nature of the product was confirmed by X-ray diffraction (Fig. S2 in the Electronic Supplementary Material).

All chemicals used for sample preservation, analysis and reagent preparation were analytical grade or higher. Ultrapure water (18 MΩ cm^{-1}, Milli-Q Advantage, Molsheim, France) was used for all solutions and dilutions.

Colloidal suspensions

Colloidal suspensions obtained by leaching of an As-rich mine waste were studied (the origin of the mine waste and its physical and chemical characteristics are described in the Electronic Supplementary Material). Mine waste samples were leached following the protocol described elsewhere [14], with the modifications shown in the Fig. 1 in order to obtain colloidal suspensions containing particles below ca. 1 μm and dissolved species. Briefly, 4 g of mine waste were mixed with 40 mL of leaching solution (1 mM KCl), placed into acid pre-cleaned polyethylene tubes and agitated in a rotary tumbler at a speed of 28±2 rpm at room temperature. Four leaching conditions, varying pH and time, were studied: (i) pH 3, t=24 h; (ii) pH 3, t=168 h; (iii) pH 6, t=6 h; (iv) pH 6, t=168 h (pH was checked at 6 h, 12 h and every 24 h, adjusting it with HNO_3 or KOH 0.1 M if necessary). Suspensions were centrifuged (Heraeus Multifuge X1R equiped with swing bucket rotor 75003629, Thermo Fisher Scientific, Walthman, USA) at 800 rpm for 11 min to remove particles larger than ca. 1 μm [14]. The resulting supernatant solutions (~20 mL), containing particles below 1 μm along with dissolved species, were analyzed by HR-ICP-MS, SP-ICP-MS and TEM, within the following 48 h. Additionally, the colloidal fractions were separated from the suspensions by ultrafiltration using 100 kDa (ca. 10 nm pore size) polyether sulfone membranes

(Microsep, Pall, Ann Arbor, USA). The colloids retained onto the membranes were analyzed by XAS.

Total element concentration

Ten mililiters of each colloid suspensions were dissolved in aqua regia and subjected to microwave-assisted digestion (Ethos Series 1, Milestone, Milan, Italy). The solutions from the digestion were filtered and analyzed for As and Fe by high resolution-inductively coupled plasma-mass spectrometer (HR-ICP-MS, Thermo Scientific Element XR, Walthman, USA).

Ultrafiltration

Dissolved As in the colloidal suspensions was separated by ultrafiltration through polyether sulfone membranes with 3 kDa pore size (Nanosep, Pall, Ann Arbor, USA). To this end, 300 µL of each suspension in duplicate were added to the ultrafiltration cartridge and centrifuged at 9000 rpm for 15 minutes. The ultrafiltrate was diluted to 10 mL before performing the ICP-MS analysis.

Single-particle ICP-MS analysis

A Perkin-Elmer Sciex model DRC-e ICP mass spectrometer (Toronto, Canada) was used for SP-ICP-MS analyses. The sample introduction system consisted of a glass concentric Slurry nebulizer and a cyclonic spray chamber (Glass Expansion, Melbourne, Australia). Default instrumental and data acquisition parameters are listed in Table 1. Data obtained with ICP-MS software (ELAN instrument software version 3.3) were imported as comma delimited files into Excel (Microsoft, Redmond, USA) and Origin

8.0 data analysis software (OriginLab Corporation, Northampton, MA, USA) and further processed.

The mass of arsenic per particle (m_P) was determined according the following expression [16]:

$$r_P = K_{ICPMS} K_M m_P \qquad \text{equation 1}$$

where r_P is the pulse intensity (measured in counts), K_{ICPMS} the detection efficiency (ratio of the number of ions detected versus the number of atoms introduced into the ICP) and K_M (= AN_{Av}/M_M) includes the contribution from the element measured (A, atomic abundance of the isotope considered, 1 for As; N_{Av}, Avogadro number; M_M, the atomic mass of As). K_{ICPMS} was estimated following a procedure based on the use of dissolved standards of the element and the nebulization efficiency of the instrument [~~24~~25]. Briefly, the relationship between the signal r (ions counted) and the mass concentration of a solution of an element M (C_M), which is nebulized into an ICP-MS, can be expressed as [16]:

$$r_{dis} = K_{int\,r} K_{ICPMS} K_M t_{dwell} C_M \qquad \text{equation 2}$$

where r_{dis} is the signal intensity (counts), K_{intr} (= $\eta_{neb} Q_{sam}$) represents the contribution from the sample introduction system, through the nebulization efficiency (η_{neb}) and the sample uptake rate (Q_{sam}), and t_{dwell} the dwell time. The mass of element (m_{dis}) measured from the solution of concentration C_M along a dwell time (t_{dwell}) is given by:

$$m_{dis} = \eta_{neb} Q_{sam} t_{dwell} C_M \qquad \text{equation 3}$$

By combining equations 2 and 3:

$$r_{dis} = K_{ICPMS} K_M m_{dis} \qquad \text{equation 4}$$

which is equivalent to equation 1, if the element behaves in a similar way both in particulate or dissolved form. Application of equation 1 requires knowledge of the detection efficiency for the instrument and the element selected. K_{ICPMS} can be obtained

by performing a calibration with dissolved standards (equation 2), once the nebulization efficiency, the sample flow rate, the dwell time and the factor K_M are known. Nebulization efficiency was calculated following the particle frequency method developed by Pace et al. [25], as the ratio between the number of particles detected and nebulized, by using a suspension of known number concentration prepared from NIST RM8013 60 nm gold nanoparticles.

X-ray absorption spectroscopy

Colloidal fractions isolated by the procedure described above were analyzed by X-ray absorption spectroscopy (XAS). Arsenic and Fe K-edge EXAFS spectra were collected at the bending magnet BM25A beamline at the European Synchrotron Radiation Facility (ESRF, Grenoble, France). Methods and reference materials (table S1) are described in the Electronic Supplementary Material.

Transmision electron microscopy

A JEOL JEM 2100 (JEOL Ltd., Tokyo, Japan) transmission electron microscope was used with an operating voltage of 200 kV. Colloidal suspensions were deposited on carbon-coated Ni grids and evaporated. Energy-dispersive X-ray spectrometry (EDS) was performed with the attached OXFORD INCA system. Image processing was performed using Image J software (U.S. National Institute of Health, Bethesda, Maryland, USA) [26].

RESULTS AND DISCUSSION

Release of arsenic from contaminated mine wastes

Previous studies of the bulk mine wastes by XAS and XRD showed that arsenic was mainly present as scorodite, whereas in the soils and sediments surrounding the dump area arsenic was found to be associated with ferrihydrite (hydrous ferric oxyhydroxide) [7]. Colloidal suspensions leached from these samples were analyzed by asymmetrical flow field flow fractionation ICP-MS (AF4-ICP-MS) and XAS. These results confirmed that arsenic was sorbed onto colloidal ferrihydrite particles, with sizes between tens to hundreds of nanometers depending on the sample type [15]. On the other hand, suspensions from the mine wastes could not be analyzed directly by AF4-ICP-MS, due to their acidic pH and high ionic strength, which led to the aggregation and adsorption of the colloids inside the separation channel of the AF4 system.

Although scorodite has been proposed as a phase for removing dissolved arsenic due to its low solubility and long-term stability, scorodite mobilization as colloidal particles and potential dissolution with changing environmental conditions cannot be ruled out. In the area under study, pH of soil samples ranged from 3.3 in the mine waste pile to 6.1 in the sediment from a pond where the surface runoff from the waste pile was collected. To mimic the pH range observed at field site, soil leaching experiments were performed at pH 3 and 6 which includes the pH of minimum solubility of scorodite (3-4) [27]. Solutions of 1 mM KCl were used as the leaching medium in order to simulate the ionic strength of runoff and superficial waters. Because scorodite dissolution is expected to be extremely slow [~~27~~28], leaching times up to 7 days were selected. In addition, a synthetic scorodite was used as a control sample for As-bearing particulate material.

Table 2 shows the total arsenic and iron concentrations in the colloidal suspensions leached from the mine waste soils for the four leaching conditions selected. Arsenic

concentrations ranged from 2.74 to 4.38 mg L^{-1}. The suspensions showed an As/Fe molar ratio close to 1, consistent with the presence of scorodite.

The fraction of arsenic leached from the soil in dissolved form was determined by ultrafiltration of the colloidal suspensions using 3 kDa cartridges. The pore size of the membranes is ca. 1 nm, and thus the ultrafiltrate was assumed to contain only dissolved arsenic species, mainly arsenate. The potential adsorption of dissolved arsenic on the PES ultrafiltration membrane was checked by ultrafiltration of standard solutions of arsenate (50 μg L^{-1}). Recoveries of 99.7 ± 0.5 and 99.0 ± 0.9 were obtained at pH 3 and 6, respectively, showing that no significant adsorption of ionic arsenate occurs on the PES membrane. Table 3 summarizes the colloidal fraction of arsenic present in the suspensions studied and in the synthetic scorodite control. This colloidal fraction was calculated as the difference between the total concentration of arsenic in the suspensions and the concentration determined in the ultrafiltrates, corresponding to arsenic associated with particles between 1 nm and 1 μm. Clearly, around 90% of arsenic is leached as colloidal particles both at pH 3 and 6, and even for the synthetic scorodite, at short leaching times. After 7 days, the colloidal fraction was reduced slightly (to 86%) at pH 3 and more significantly (to 72%) at pH 6. These results suggest that steady-state conditions were achieved at pH 3 between 1 and 7 days, whereas dissolution of colloidal arsenic species or the release of ionic arsenic from colloidal particles occurred at pH 6.

Detection of arsenic-bearing particles by SP-ICP-MS

Ultrafiltration in combination with an atomic spectrometry technique (ICP-MS) provided indirect evidence about the presence of arsenic associated with colloidal particles released from the mine waste sample. However, analysis of the colloidal

suspensions by SP-ICP-MS can provide direct evidence about the arsenic-bearing particles. Suspensions of the synthetic scorodite were used as a reference for As-bearing particles. Fig. 2a shows a typical SP-ICP-MS time scan obtained from a synthetic scorodite suspension with a total arsenic concentration of 50 $\mu g\ L^{-1}$. By plotting the corresponding frequency histograms (Fig. 2b), two partially overlaped distributions were obtained. The first distribution was due to the background and the marginal contribution of dissolved arsenic, and the second distribution corresponds to the As-bearing particles. Two resolved distribution were not obtained due to the attainable mass-per-particle limit of detection (LOD_{mass}). Based on a 3σ criterion, this limit of detection can be expressed as:

$$LOD_{mass} = \frac{3\sigma_B}{K_{ICPMS}K_M} \qquad \text{equation 5}$$

where K_{ICPMS} is the detection efficiency (ratio of the number of ions detected versus the number of atoms introduced into the ICP), and K_M ($= AN_{Av}/M_M$) includes the contribution from the element measured, where A is the atomic abundance of the isotope considered, N_{Av} the Avogadro number and M_M the atomic mass of M [16]. For arsenic and the experimental conditions used here, a LOD_{mass} of 0.64 ng per particle could be achieved.

The data from the histogram of Fig. 2b was processed according the protocol developed by Laborda et al. [16]. The pulse intensity corresponding to the mode of the first distribution (μ_B) was used for calculating the threshold criterion ($S_C = \sqrt{\mu_B + 1}$) for removal of background events, as well as for subtracting the particle events to obtain their corresponding net intensities. Pulse intensities were converted to arsenic masses, by using equation 1, in order to obtain the corresponding mass-per-particle histogram (Fig. 2c).

Fig. 3 shows the mass-per-particle histograms corresponding to the colloidal suspensions leached from the mine waste. The histograms provide direct evidence of arsenic associated with particles from soil leaching, but not about the nature of such particles.Additional characterization techniques are needed to determine the specific composition of the particles and to relate the mass-per-particle content to the size of the particles.

Speciation of As in the colloidal fraction by XAS

The As and Fe K-edge EXAFS spectra of the colloidal fraction leached from the mine waste and results of linear combination fits (LCF) of reference As and Fe compounds are shown in Fig. 4; fit results are repored in Table 4. The As K-edge EXAFS spectra indicates a major contribution from scorodite (67 – 86%), and a secondary contribution from As(V) sorbed to ferrihydrite (18 – 33%). The corresponding Fe K-edge EXAFS spectra were also characterized by a major contribution from scorodite (86 – 92%) and a minor fraction of a Fe-oxide phase such as hematite or goethite (13 – 16%). Both As and Fe EXAFS spectra point out the decreasing contribution of scorodite with time after the leaching experiments. The EXAFS spectra of the colloidal fractions were also analyzed shell-by-shell to determine interatomic distances . (Tables S2 and S3, Electronic Supplementary Material). Fit results showed that As and Fe atomic environments in the colloids were consistent with a dominant fraction of As and Fe in scorodite [29,30]. X-ray absorption spectroscopy analysis confirmed that arsenic is mostly leached from the contaminated soil as particles of scorodite.

Size determination of As-bearing particle

Once the composition and phase of the arsenic-bearing particles are known, the size of the particles can be estimated. Scorodite crystals present an orthorhombic structure (Fig. ~~9~~S3 in the Electronic Supplementary Material), corresponding to FeO_6 octahedra sharing corners with four adjacent arsenate tetrahedra (AsO_4) in a three-dimensional framework [30,31] with a rhombic dipiramidal form. Assuming that the three edges of the rhombic dipiramide are equal to e (fig. S3 in Supplementary Electronic Material), the mass of arsenic per particle (m_{As}) can be related to the edge through:

$$m_{As} = \frac{\sqrt{2}}{3} 10^{-21} \rho X_{As} e^3 \qquad \text{equation 6}$$

where ρ is the density of the scorodite (3.27 g cm^{-3}), X_{As} the mass fraction of arsenic in scorodite (74.92/230.79).

Using the equation 6, a size limit of detection (LOD_{size}), related to the average edge of scorodite crystals, can be estimated from the previously calculated LOD_{mass}. Assuming that arsenic is found in the particles as scorodite, and using the experimental conditions of this work, a LOD_{size} of 117 nm could be achieved.

Equation 6 was used to transform mass-per-particle histograms (Fig. 2c and 3) into size histograms. Fig. 2d shows the size histogram corresponding to synthetic scorodite, and size histograms of the colloidal particles from the mine waste are presented in Fig. 5.

Fig. 2 shows all of the steps required to obtain size information from a suspension by SP-ICP-MS. Once the time scan has been acquired (Fig. 2a), the signal histogram is plotted (Fig. 2b). Next, the background contribution is removed, and the signal intensities corresponding to particle events are converted to mass of the target element by using equation 1 (Fig. 2c). Finally, mass-per-particle histograms are converted into

size histograms through equation 6 (Fig. 2d). The synthetic scorodite showed sizes below 200-250 nm.

Size histograms from Fig. 5 reveal that arsenic is mobilized from the mine waste as scorodite particles with sizes up to 300-350 nm for leaching times of 24 hours. The size of the particles decreases to 250-300 nm for leaching times of 7 days, suggesting some dissolution of scorodite with time, particularly at pH 6. Due to the size limit of detection determined above (117 nm), particle size distributions between 10-100 nm could not be measured.

Colloidal suspensions were also analyzed by TEM-EDS to confirm the results obtained by SP-ICP-MS. In all samples, orthorhombic structures with an As/Fe molar ratio close to 1 were observed, consistent with the presence of scorodite particles. By further processing of the images, scorodite crystals below 300-350 nm were observed, (Fig. 6), in agreement with the size information obtained by SP-ICP-MS.

CONCLUSIONS

SP-ICP-MS is capable of providing direct evidence about the presence of elements in particulate form in suspensions, as well as information about the mass of element per particle. However, SP-ICP-MS cannot give information about the size of the particles unless supplemented with additional information about their composition, shape and density in order to transform mass-per-particle into size information. The composition of engineered nanoparticles is usually known, but this is uncommon for natural colloids in environmental samples that often contain heterogeneous mixtures. In such cases, additional information about the speciation of the element is required. By combining SP-ICP-MS, that provided specific information about particulate forms of arsenic, and XAS, that allowed to know the speciation of the particles, direct evidence of the

leaching of arsenic from a mine waste as scorodite particles with sizes below 300-350 nm was obtained. TEM analysis also supported the size determination of the As-bearing particles leached.

The approach described involves that particles bearing the element under study should be present as just one major chemical species to obtain size information from the SP-ICP-MS measurements. Furthermore, the possibility of obtaining full particle size distributions relies on size detection limits low enough, which in turn depend on the element monitored, the composition of the particles involved and the detection efficiency of the ICP-MS instrument used. This means that better performance may be achieved by using double focusing or improved quadrupole or time-of-flight instruments. Finally, although along this work XAS has been used to obtain the speciation information required, other characterization techniques may be applied, like bulk X-ray diffraction or TEM combined with selected area electron diffraction (SAED) and/or electron energy loss spectroscopy (EELS).

Acknowledgements

The SP-ICP-MS analyses were performed at Servicio de Análisis Químico (Servicio General de Apoyo a la Investigación-SAI), Universidad de Zaragoza. The HR-ICP-MS analyses were performed at the LabGEOTOP service, ICTJA-CSIC.

Funding

This work was supported by the Spanish Ministry of Economy and Competitiveness under the research projects: CGL2010-17434 and CTQ2012-38091-C02-01.

The XAS measurements on the BM25A beamline (European Synchrotron Radiation Facility) were supported by the project 25-01-849 of the ESRF.

Conflicts of interest

M.A. Gomez-Gonzalez was supported by the PhD fellowship program FPI (BES-2011-046461) and additionally granted through the aid for the performance of short stays abroad by the program for graduate students (EEBB-I-13-06505) from the Spanish Ministry of Economy and Competitiveness.

The other authors of this work declare that they have no conflict of interest.

REFERENCES

1. Kretzschmar R, Sticher H. Transport of Humic-Coated Iron Oxide Colloids in a Sandy Soil: Influence of Ca2+ and Trace Metals. Environmental Science & Technology 1997;31:3497-3504.

2. Hassellov M, von der Kammer F. Iron Oxides as Geochemical Nanovectors for Metal Transport in Soil-River Systems. Elements 2008;4:401-406.

3. Root RA, Vlassopoulos D, Rivera NA, Rafferty MT, Andrews C, O'Day PA. Speciation and natural attenuation of arsenic and iron in a tidally influenced shallow aquifer. Geochimica et Cosmochimica Acta 2009;73:5528-5553.

4. Slowey AJ, Johnson SB, Newville M, Brown GE. Speciation and colloid transport of arsenic from mine tailings. Applied Geochemistry 2007;22:1884-1898.

5. Paktunc D, Dutrizac J, Gertsman V. Synthesis and phase transformations involving scorodite, ferric arsenate and arsenical ferrihydrite: Implications for arsenic mobility. Geochimica et Cosmochimica Acta 2008;72:2649-2672.

6. Flemming RL, Salzsauler KA, Sherriff BL, Sidenko NV. Identification of scorodite in fine-grained, high-sulfide, arsenopyrite mine-waste using micro X-ray diffraction (μ XRD). Canadian Mineralogist 2005;43:1243-1254.

7. Gomez-Gonzalez MA, Serrano S, Laborda F, Garrido F. Spread and partitioning of arsenic in soils from a mine waste site in Madrid province (Spain). Science of the Total Environment 2014;500–501:23-33.

8. Gomez-Gonzalez MA, Voegelin A, Garcia-Guinea J, Bolea E, Laborda F, Garrido F. Colloidal mobilization of arsenic from mining-affected soils by surface runoff. Chemosphere 2016; 144:1123-1131.

9. Grout H, Wiesner MR, Bottero J-Y. Analysis of Colloidal Phases in Urban Stormwater Runoff. Environmental Science & Technology 1999; 33:831-839.

10. Fritzsche A, Rennert T, Totsche KU. Arsenic strongly associates with ferrihydrite colloids formed in a soil effluent. Environmental Pollution 2011;159:1398-1405.

11. Bauer M, Blodau C. Arsenic distribution in the dissolved, colloidal and particulate size fraction of experimental solutions rich in dissolved organic matter and ferric iron. Geochimica Et Cosmochimica Acta 2009;73:529-542.

12. Plathe KL, von der Kammer F, Hassellov M, Moore J, Murayama M, Hofmann T, Hochella MF. Using FlFFF and aTEM to determine trace metal-nanoparticle associations in riverbed sediment. Environmental Chemistry 2010;7:82-93.

13. Neubauer E, von der Kammer F, Knorr KH, Peiffer S, Reichert M, Hofmann T. Colloid-associated export of arsenic in stream water during stormflow events. Chemical Geology 2013;352:81-91.

14. Bolea E, Laborda F, Castillo JR. Metal associations to microparticles, nanocolloids and macromolecules in compost leachates: Size characterization by asymmetrical flow field-flow fractionation coupled to ICP-MS. Analytica Chimica Acta 2010;661:206-214.

15. Serrano S, Gomez-Gonzalez MA, O'Day PA, Laborda F, Bolea E, Garrido F. Arsenic speciation in the dispersible colloidal fraction of soils from a mine-impacted creek. Journal of Hazardous Materials 2015;286:30-40.

16. Laborda F, Jimenez-Lamana J, Bolea E, Castillo JR. Selective identification, characterization and determination of dissolved silver(I) and silver nanoparticles based on single particle detection by inductively coupled plasma mass spectrometry. Journal of Analytical Atomic Spectrometry 2011;26:1362-1371.

17. Mitrano DM, Lesher EK, Bednar A, Monserud J, Higgins CP, Ranville JF. Detecting nanoparticulate silver using single-particle inductively coupled plasma-mass spectrometry. Environmental Toxicology and Chemistry 2012;31:115-121.

18. Laborda F, Jimenez-Lamana J, Bolea E, Castillo JR. Critical considerations for the determination of nanoparticle number concentrations, size and number size distributions by single particle ICP-MS. Journal of Analytical Atomic Spectrometry 2013;28:1220-1232.

19. Hadioui M, Merdzan V, Wilkinson KJ. Detection and Characterization of ZnO Nanoparticles in Surface and Waste Waters Using Single Particle ICPMS. Environmental Science & Technology 2015;49:6141–6148.

20. Degueldre C, Favarger PY, Wold S. Gold colloid analysis by inductively coupled plasma-mass spectrometry in a single particle mode. Analytica Chimica Acta 2006;555:263-268.

21. Degueldre C, Favarger PY. Colloid analysis by single particle inductively coupled plasma-mass spectroscopy: a feasibility study. Colloids and Surfaces A: Physicochemical and Engineering Aspects 2003;217:137-142.

22. Degueldre C, Favarger PY, Bitea C. Zirconia colloid analysis by single particle inductively coupled plasma–mass spectrometry. Analytica Chimica Acta 2004;518:137-142.

23. Voegelin A, Weber FA, Kretzschmar R. Distribution and speciation of arsenic around roots in a contaminated riparian floodplain soil: Micro-XRF element mapping and EXAFS spectroscopy. Geochimica et Cosmochimica Acta 2007;71:5804-5820.

24. Hsu PH, Sikora F. Effects of aluminum and phosphate concentrations and acidity on the crystallization of variscite at 90 °C. Soil Science 1993;156:71-78.

25. Pace HE, Rogers NJ, Jarolimek C, Coleman VA, Higgins CP, Ranville JF. Determining Transport Efficiency for the Purpose of Counting and Sizing Nanoparticles via Single Particle Inductively Coupled Plasma Mass Spectrometry. Analytical Chemistry 2011;83:9361-9369.

26. Cai Z, Vallis KA, Reilly RM. Computational analysis of the number, area and density of γ -H2AX foci in breast cancer cells exposed to 111In-DTPA-hEGF or γ -rays using Image-J software. International Journal of Radiation Biology 2009;85:262-271.

27. Paktunc D, Bruggeman K. Solubility of nanocrystalline scorodite and amorphous ferric arsenate: Implications for stabilization of arsenic in mine wastes. Applied Geochemistry 2010;25:674-683.

28. Bluteau MC, Demopoulos GP The incongruent dissolution of scorodite - Solubility, kinetics and mechanism. Hydrometallurgy 2007;87:163-177.

29. Kitahama K, Kiriyama R, Baba Y. Refinement of crystal-structure of scorodite. Acta Crystallographica Section B-Structural Science 1975;31:322-324.

30. Mikutta C, Mandaliev PN, Kretzschmar R. New Clues to the Local Atomic Structure of Short-Range Ordered Ferric Arsenate from Extended X-ray Absorption Fine Structure Spectroscopy. Environmental Science & Technology 2013;47:3122-3131.

31. Neil CW, Yang YJ, Jun YS. Arsenic mobilization and attenuation by mineral-water interactions: implications for managed aquifer recharge. Journal of Environmental Monitoring 2012;14:1772-1788.

Table 1 Default instrumental and data acquisition parameters

Instrumental parameters of ICP-MS		
RF power	1200 W	
Argon gas flow rate		
Plasma	15 L min^{-1}	
Auxiliary	1.2 L min^{-1}	
Nebulizer	1.0 L min^{-1}	
Sample uptake rate	1.0 mL min^{-1}	
Data acquisition parameters of ICPMS		
Measuring mode	Standard	Single particle detection
Points per spectral peak	1	1
Sweeps	20	1
Dwell time	50 ms	5 ms
Readings per replicate	1	12000
Settle time	3 ms	3 ms
Integration time	1 s	60 s

Table 2 Total arsenic and iron concentrations of colloidal suspensions leached from the mine waste under different leaching conditions measured by HR-ICP-MS (mean± standard deviation, *n=3*)

pH	Leaching time	As	Fe	As/Fe molar ratio
		mg L^{-1}		
3	24 h	2.74 ± 0.12	2.06 ± 0.11	1.01
	168 h	2.84 ± 0.07	2.09 ± 0.14	1.03
6	6 h	4.38 ± 0.18	3.61 ± 0.32	0.89
	168 h	3.39 ± 0.07	2.35 ± 0.14	1.09

Table 3 Colloidal fraction of arsenic in synthetic scorodite and colloidal suspensions leached from the mine waste under different leaching conditions [a]

Sample	pH	Time h	As colloidal fraction %
Synthetic Scorodite	3	24	91 ± 1
	6	24	91 ± 2
Mine waste	3	24	89 ± 2
	3	168	86 ± 3
	6	6	93 ± 1
	6	168	72 ± 3

[a] *Calculated as the difference between the ICP-MS analysis of As before and after ultrafiltrating the samples by 3 kDa membranes, ± standard deviation of three replicate experiments*

Table 4 Linear combination fit results using reference compound spectra for As and Fe K-edge EXAFS spectra of the colloidal fraction leached from the mine waste under different leaching conditions [a].

As EXAFS [b]					
Sample	**Scorodite** [c] **%**	**As sorbed to Ferrihydrite** [c] **%**	**Total %**	**R factor** [d]	**red χ^2** [e]
pH 3, 168 h	67.4	35.8	103.2	0.0285	0.7373
pH 6, 6 h	86.2	17.9	104.1	0.0248	0.8285
pH 6, 168 h	80.5	21.4	101.9	0.0225	0.6650
Fe EXAFS [f]					
Sample	**Scorodite** [b] **%**	**Fe-oxide** [g] **%**	**Total %**	**R factor** [d]	**red χ^2** [e]
pH 3, 168 h	87.3	16.1	103.4	0.0750	0.9091
pH 6, 6 h	92.4	13.0	105.4	0.0556	0.6724
pH 6, 168 h	85.8	15.9	101.7	0.0636	0.734

[a] *Fitting percentages were not constrained to sum 100 %*
[b] *LCF EXAFS range for As: 2 – 12.5 Å, spectra measured at ESRF (Grenoble, France)*
[c] *More details about reference spectrum was summarized in the Electronic Supplementary Material (Table S1)*
[d] *Normalized sum of the squared residuals of the fit [$R = \sum(data-fit)^2 / \sum data^2$)]*
[e] *Goodness-of-fit was assessed by the χ^2 statistic [= (F factor) / (no. of points – no. of variables)]*
[f] *LCF EXAFS range for Fe: 2 – 11 Å, spectra measured at ESRF (Grenoble, France)*
[g] *The short k-range of the Fe spectra causes that the LCF's are not unique, matching with both Hematite and Goethite standards. The parameters showed in the Table are the ones corresponding to the Hematite standard*

FIGURE CAPTIONS

Fig 1 Procedure for the isolation of the colloidal samples from the mine waste and the analyses performed on the colloidal suspension (≤ 1 µm), the colloidal fraction (1 µm - 10 nm) and the dissolved fraction (< 1 nm).

Fig 2 (a) ^{75}As time scan of colloidal suspensions (≤ 1 µm) from the synthetic scorodite. (b) Signal distribution histogram obtained from the (a) time scan. First distribution (red line) corresponds to background/dissolved As, second distribution (yellow line) to colloidal As. (c) Mass-per-particle histogram. (d) Size histogram.

Fig 3 Mass-per-particle histograms of colloidal suspension (≤ 1 µm) from mine waste leachates. (a) pH 3, t=24h; (b) pH 3, t=168 h; (c) pH 6, t=6 h and (d) pH 6, t=168 h.

Fig 4 Arsenic K-edge EXAFS spectra (a) and magnitude Fourier-transformed EXAFS spectra (b) of the colloidal fractions: (ii) pH 3, t=168 h; (iii) pH 6, t=6 h and (iv) pH 6, t=168 h. Iron K-edge EXAFS spectra (c) and magnitude Fourier-transformed EXAFS spectra (d) of the colloidal fractions. Experimental data are shown as black lines and linear combination fits (LCF) are presented as red lines. Fit results are given in Table 4.

Fig 5 SP-ICP-MS histograms of the colloidal suspensions (≤ 1 µm) leached from the mine waste under different leaching conditions.(a) pH 3, t=24h; (b) pH 3, t=168 h; (c) pH 6, t=6 h and (d) pH 6, t=168 h.

Fig 6 Transmission electron microscopy (TEM) images of the colloidal suspensions (≤ 1 µm) leached from the mine waste under different leaching conditions.: (a) pH 3, t=24h; (b) pH 3, t=168 h; (c) pH 6, t=6 h and (d) pH 6, t=168 h. Dotted rectangles indicated scorodite crystals (molar As/Fe ratio ca. 1).

Figure 1

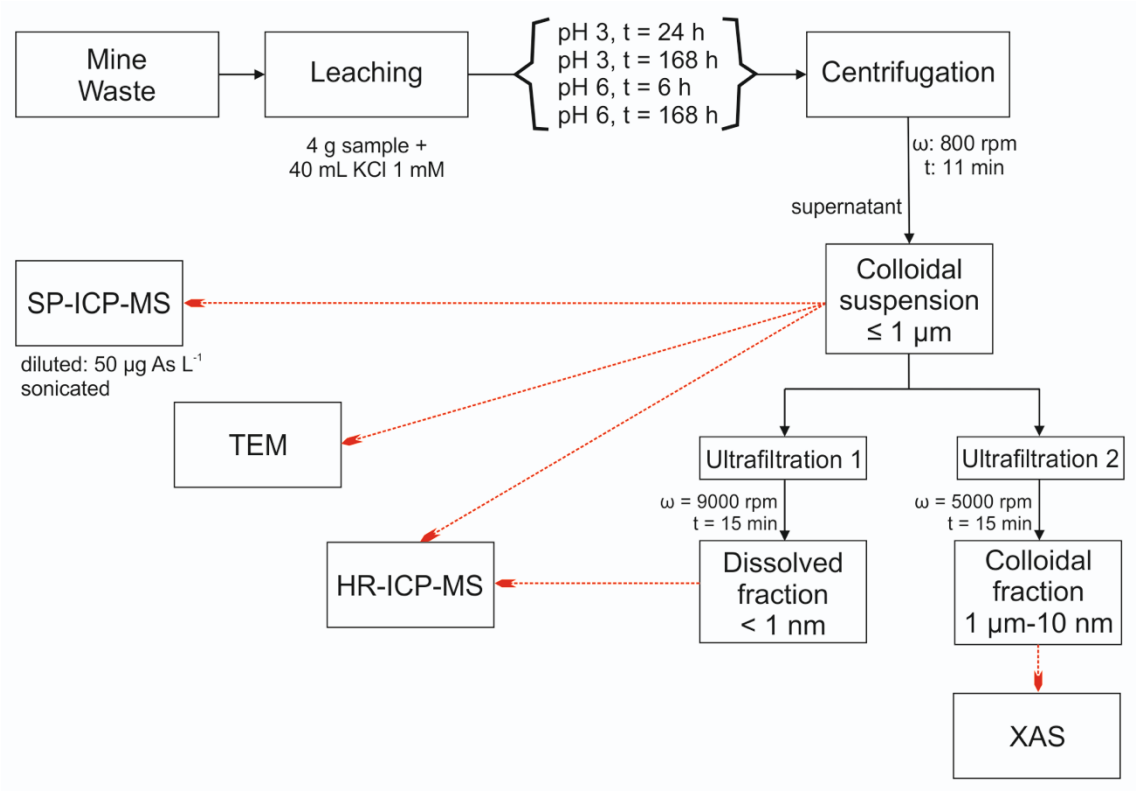
Mine Waste
Leaching
4 g sample +
40 mL KCl 1 mM
pH 3, t = 24 h
pH 3, t = 168 h
pH 6, t = 6 h
pH 6, t = 168 h
Centrifugation
ω: 800 rpm
t: 11 min
supernatant
Colloidal suspension ≤ 1 µm
SP-ICP-MS
diluted: 50 µg As L-1
sonicated
TEM
Ultrafiltration 1
ω = 9000 rpm
t = 15 min
Ultrafiltration 2
ω = 5000 rpm
t = 15 min
HR-ICP-MS
Dissolved fraction < 1 nm
Colloidal fraction 1 µm-10 nm
XAS

Figure 2

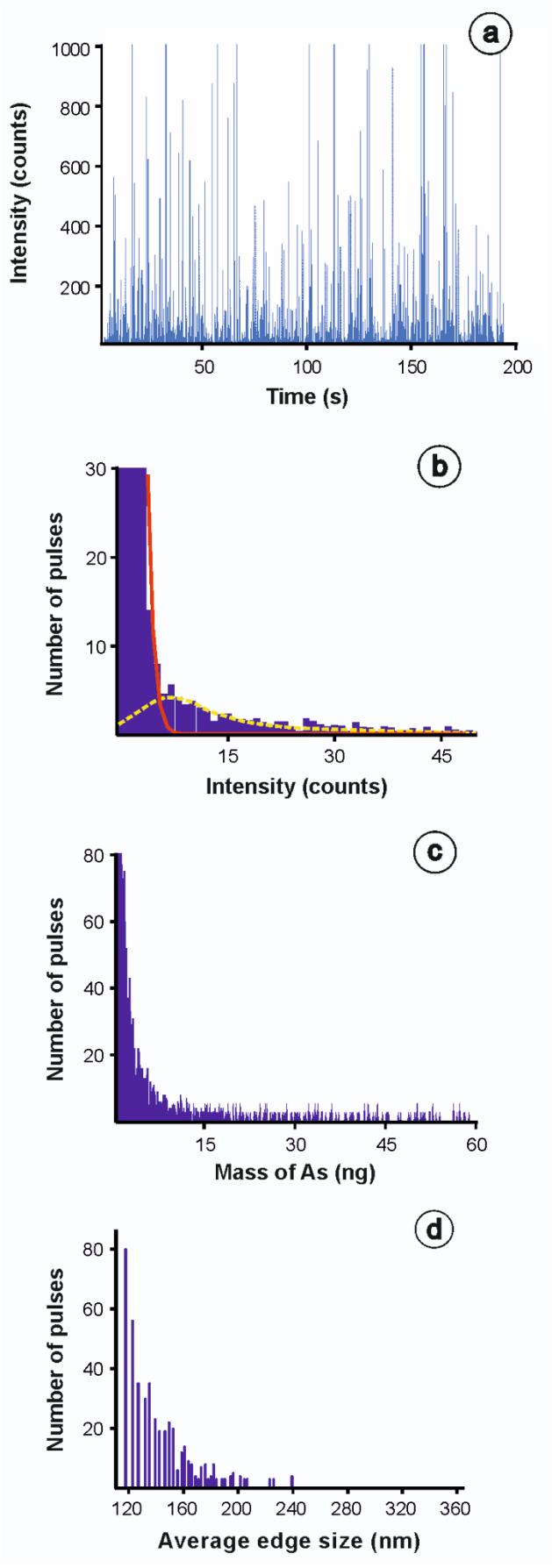
a
1000
800
600
400
200
Intensity (counts)
50
100
150
200
Time (s)
b
30
20
10
Number of pulses
15
30
45
Intensity (counts)
c
80
60
40
20
Number of pulses
15
30
45
60
Mass of As (ng)
d
80
60
40
20
Number of pulses
120
160
200
240
280
320
360
Average edge size (nm)

Figure 3

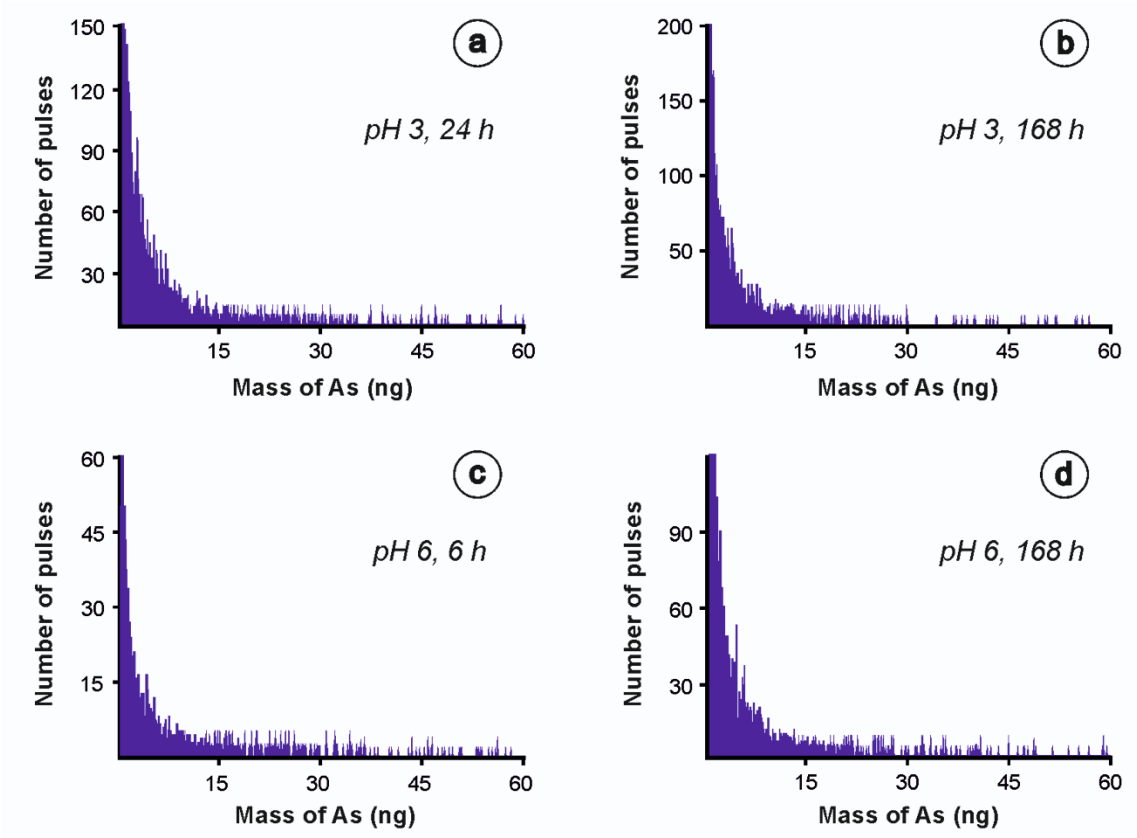
a
pH 3, 24 h
Number of pulses
150
120
90
60
30
15
30
45
60
Mass of As (ng)
b
pH 3, 168 h
Number of pulses
200
150
100
50
15
30
45
60
Mass of As (ng)
c
pH 6, 6 h
Number of pulses
60
45
30
15
15
30
45
60
Mass of As (ng)
d
pH 6, 168 h
Number of pulses
90
60
30
15
30
45
60
Mass of As (ng)

Figure 4

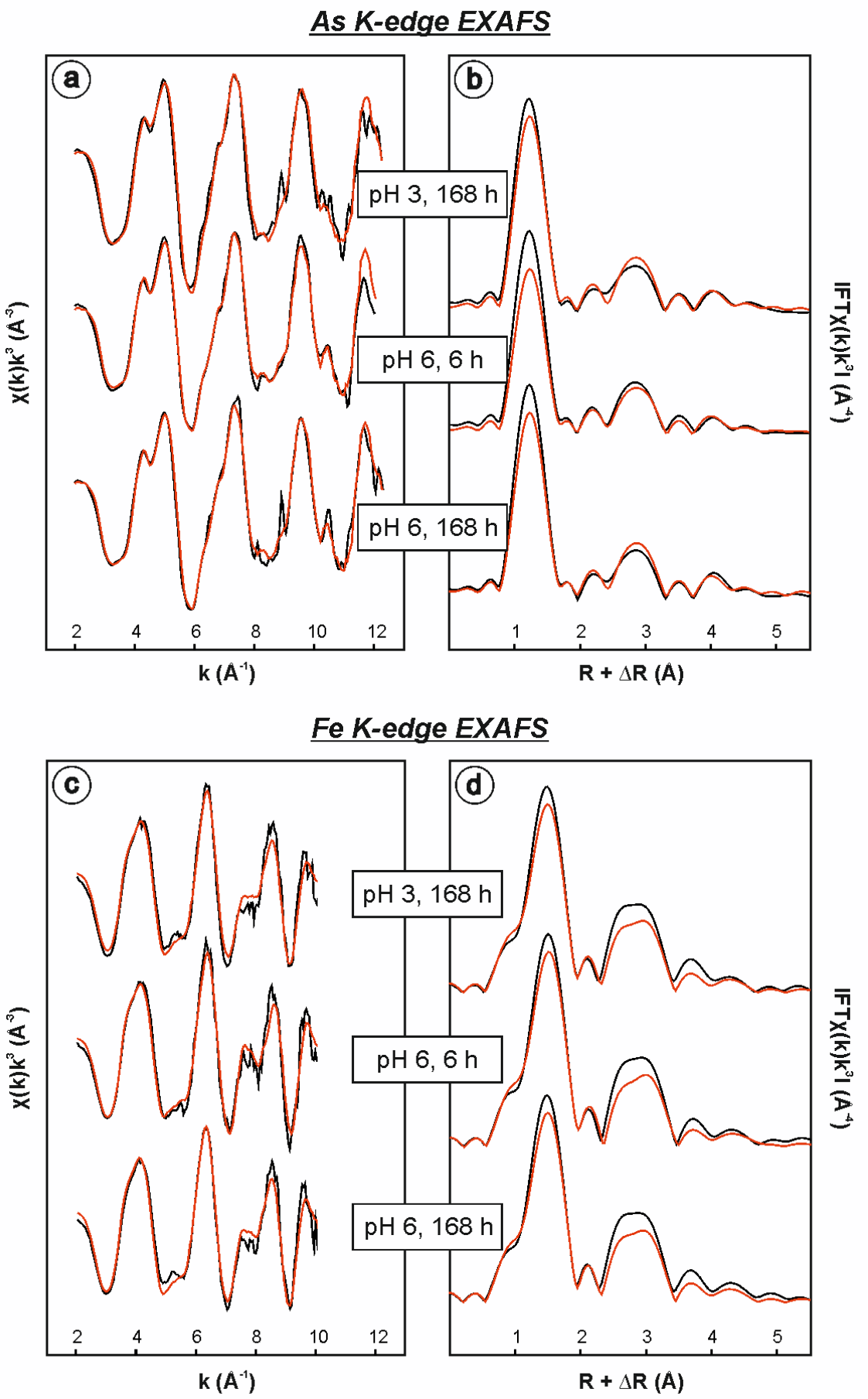
As K-edge EXAFS
a
b
pH 3, 168 h
pH 6, 6 h
pH 6, 168 h
χ(k)k³ (Å⁻³)
IFTχ(k)k³I (Å⁻⁴)
2 4 6 8 10 12
k (Å⁻¹)
1 2 3 4 5
R + ΔR (Å)
Fe K-edge EXAFS
c
d
pH 3, 168 h
pH 6, 6 h
pH 6, 168 h
χ(k)k³ (Å⁻³)
IFTχ(k)k³I (Å⁻⁴)
2 4 6 8 10 12
k (Å⁻¹)
1 2 3 4 5
R + ΔR (Å)

Figure 5

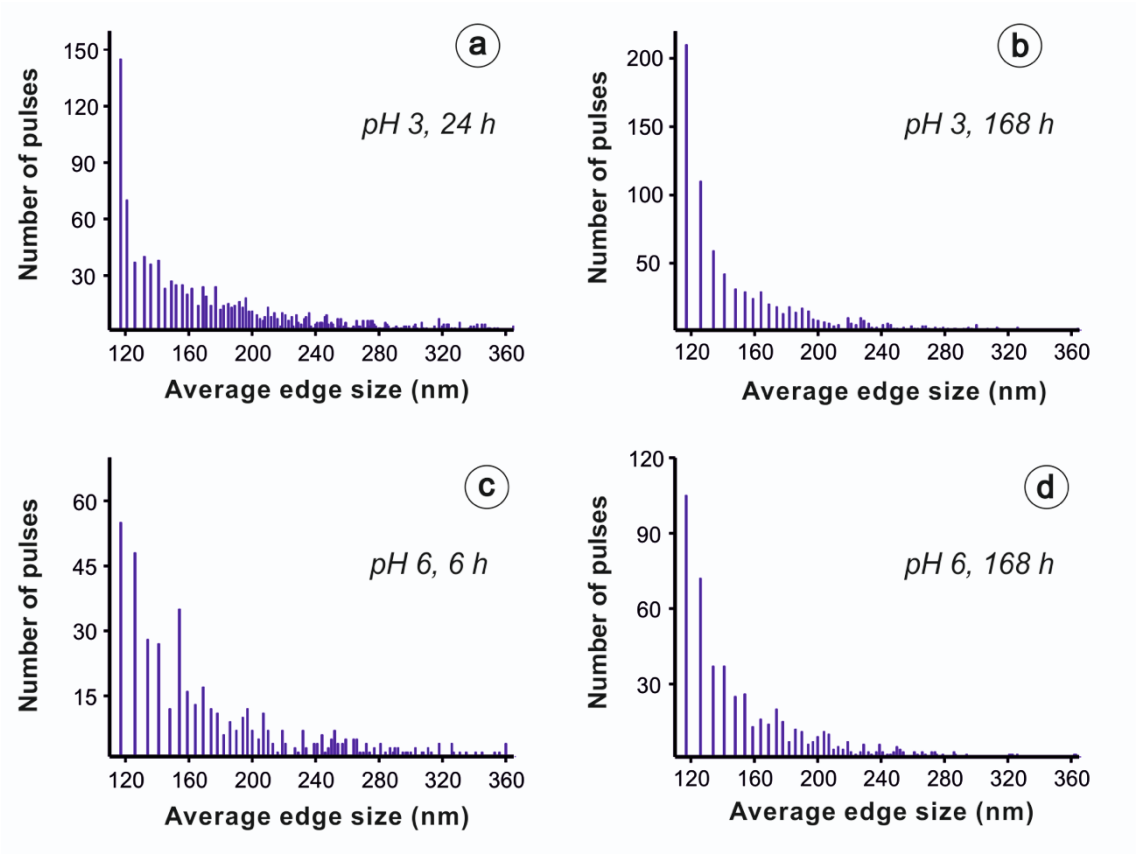
a
pH 3, 24 h
Number of pulses
150
120
90
60
30
120 160 200 240 280 320 360
Average edge size (nm)
b
pH 3, 168 h
Number of pulses
200
150
100
50
120 160 200 240 280 320 360
Average edge size (nm)
c
pH 6, 6 h
Number of pulses
60
45
30
15
120 160 200 240 280 320 360
Average edge size (nm)
d
pH 6, 168 h
Number of pulses
120
90
60
30
120 160 200 240 280 320 360
Average edge size (nm)

Figure 6

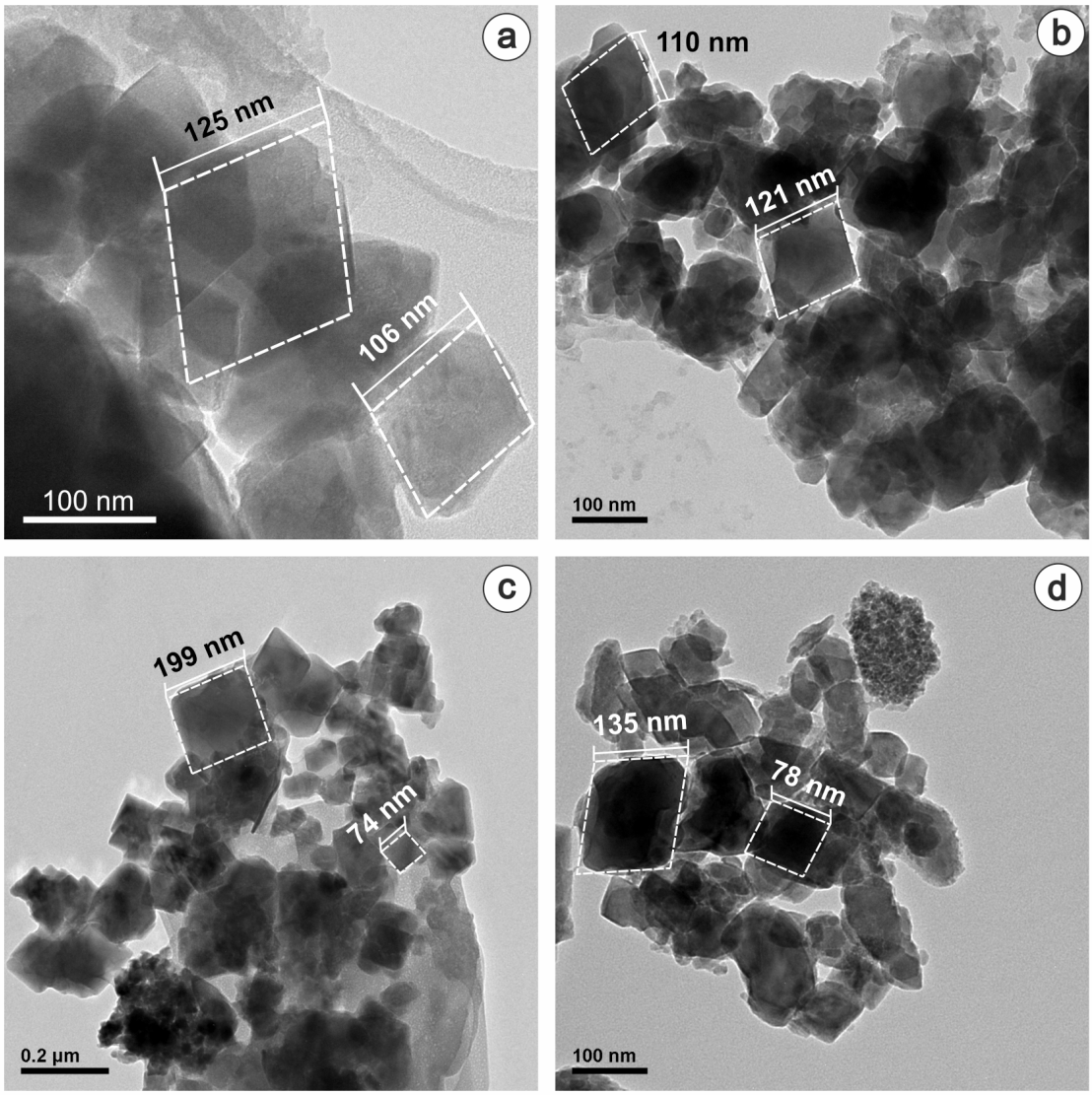
a
125 nm
106 nm
100 nm
b
110 nm
121 nm
100 nm
c
199 nm
74 nm
0.2 µm
d
135 nm
78 nm
100 nm

Supplementary Material

Combining single-particle inductively coupled plasma mass spectrometry and X-ray absorption spectroscopy to evaluate the release of colloidal arsenic from environmental samples

Miguel Angel Gomez-Gonzalez [1], Eduardo Bolea [2], Peggy A. O'Day [3], Javier Garcia-Guinea [1], Fernando Garrido [1], Francisco Laborda [2]

[1] *National Museum of Natural Sciences, CSIC, Jose Gutierrez Abascal 2, 28006 Madrid, Spain.*

[2] *Group of Analytical Spectroscopy and Sensors (GEAS), Institute of Environmental Sciences (IUCA), University of Zaragoza, Pedro Cerbuna 12, 50009 Zaragoza, Spain.*

[3] *Environmental Systems Program, University of California, Merced, CA 95343, USA*

Origin of the mine waste

In the upper portion of a small sub-catchment of the Guadalix River (Madrid, Spain), there is a shrubland which feeds into the Madrid Tertiary Detrital Aquifer. Scorodite [$FeAsO_4 \cdot 2H_2O$] is found in association with the sulfide-bearing pegmatite outcrops in this area [1,2]. This site includes an abandoned smelting factory at which arsenopyrite ores were roasted to extract silver and bismuth metals. Such sulfides, silver sulphosalts and wolframite ores were originally encapsulated in natural quartz veins, which were mined for wolfram extraction during the Second World War, including the regional mining wastes tips droppings. The mining wastes, which contain up to 19 g kg^{-1} of As, currently remain dumped on the soil surface suffering erosion and weathering processes [3]. Bulk samples were collected from the upper 10 cm of the waste-pile (WP) and were air dried, sieved (2-mm mesh) and homogeneized prior to analysis. The experimental

location as well as the physical, chemical and mineralogical properties of this bulk sample are presented in Fig. S1.

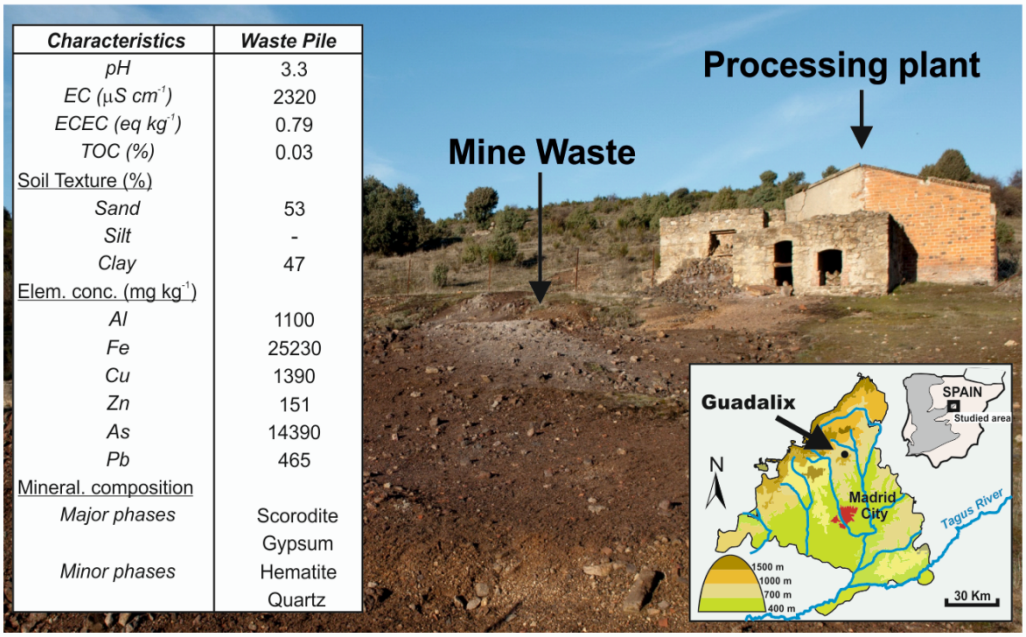

Fig S1 Location of the studied area and main physical and chemical characteristics of the bulk topsoil sample.

X-Ray diffraction analysis

Semi-quantitative mineralogical composition of the mine waste was identified by powder X-ray diffraction (XRD) with a Philips PW-1710/00 diffractometer (Eindhoven, The Netherlands) using the CuKα radiation with a Ni filter and a setting of 40 kV and 40 mA. Samples were carefully milled over a period of 15 min and pressed to produce pellets of powdered aliquots. XRD analyses were performed using XPOWDER software. Patterns were obtained by step scanning, from 3º to 65º 2θ, with a count for 0.5 s/step exploration speed of 7º/min and 40 kV and 40 mA in the X-ray tube. The qualitative search-matching procedure was based on the ICDDPDF2 and the DIFDATA databases. Synthetic scorodite was also analyzed by XRD as presented in Fig. S2.

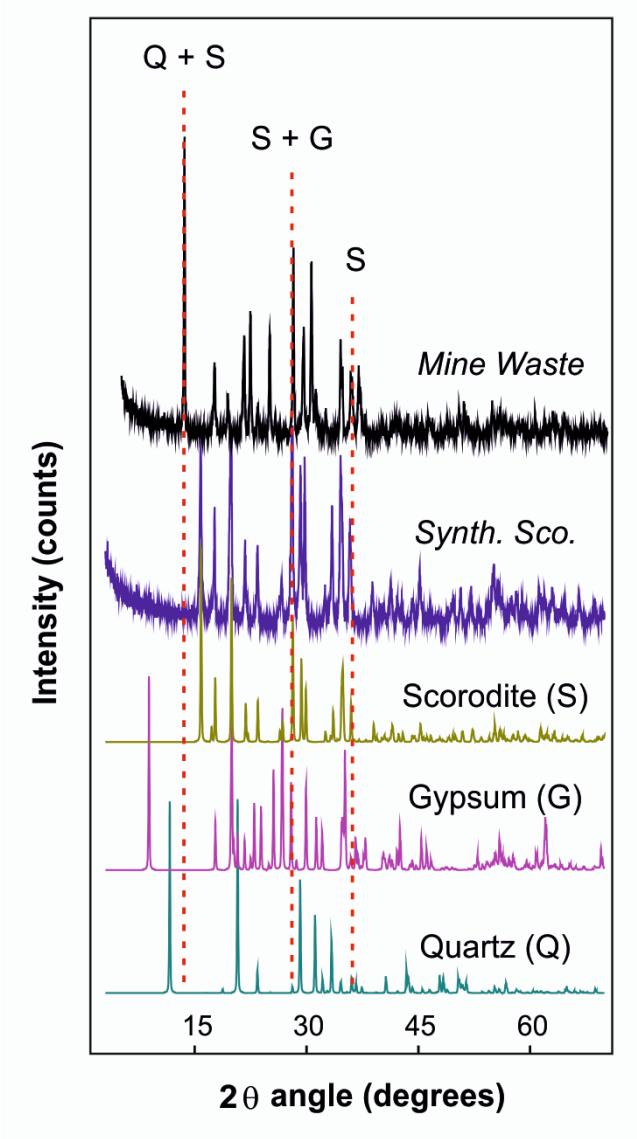

Fig S2 X-ray diffraction analyses performed on the selected remaining leaching samples and on the synthetic scorodite. Reference mineral patterns were also shown as well as the most representative peaks of the samples (red dotted lines).

Crystal structure of scorodite

The scorodite mineral ($FeAsO_4 \cdot 2H_2O$) presents an orthorhombic structure, corresponding to FeO_6 octahedra sharing corners with four adjacent arsenate tetrahedral (AsO_4) in a three dimensional framework [4]. In this work, we are trying to measure the average edge (e) in order to offer a size distribution, such as the presented in the Fig. S3.

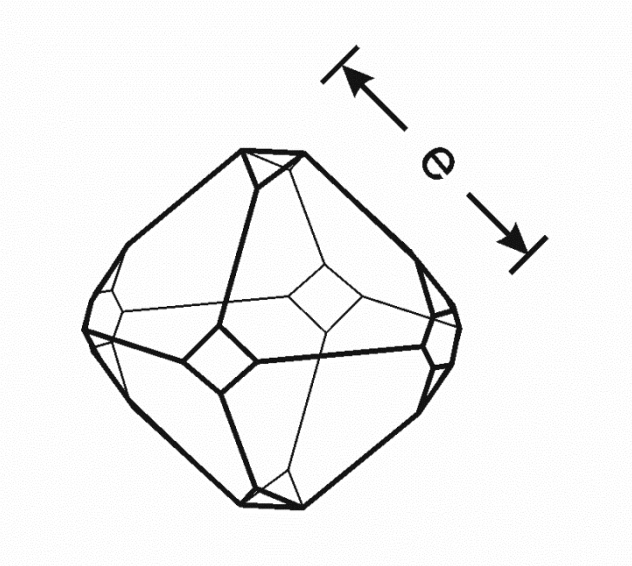

Fig S3 Orthorhombic structure corresponding to the scorodite, with the average edge size considered in this work.

As and Fe K-edge X-ray absorption spectroscopy (XAS)

The colloid-bearing ultrafiltration membranes were placed on holders made of polyether ether ketone (PEEK) material and sealed with Kapton® tape. Arsenic and Fe K-edge EXAFS spectra were recorded at the bending magnet BM25A beamline at the European Synchrotron Radiation Facility (ESRF, Grenoble, France) (6 GeV, 100 mA, Si(111) monochromator crystals) at room temperature (RT) using a 13-element Ge(Li) solid state detector. The beam energy was calibrated by setting the first inflection point in the K absorption edge of a metallic Fe foil to 7112 eV (Fe measurements) or the first maximum in the K absorption edge of KH_2AsO_4 (*Sigma-Aldrich*) to 11875 eV (As measurements). The sample spectra were acquired in fluorescence mode, starting at 6950 eV (Fe) or 11650 eV (As). The pre-edge step size was set to 5 eV, and the edge step size along the edge was set to 0.5 eV. The EXAFS spectra were collected up to 10 $Å^{-1}$ for Fe and 12.5 $Å^{-1}$ for As respectively, using a step size of 0.05 $Å^{-1}$ in k-space with

constant measurement times over the entire EXAFS range. The sample spectra were obtained by averaging several replicate scans (10-12 scans).

Both the near edge X-ray absorption spectroscopy (XANES) and the extended X-ray absorption fine structure spectroscopy (EXAFS) were analyzed. Arsenic and iron normalized K-edge XANES spectra of selected colloidal fractions were initially compared with reference compound spectra (Fig. S4). Results , showed that As was dominantly As(V) and Fe was dominantly Fe(III).

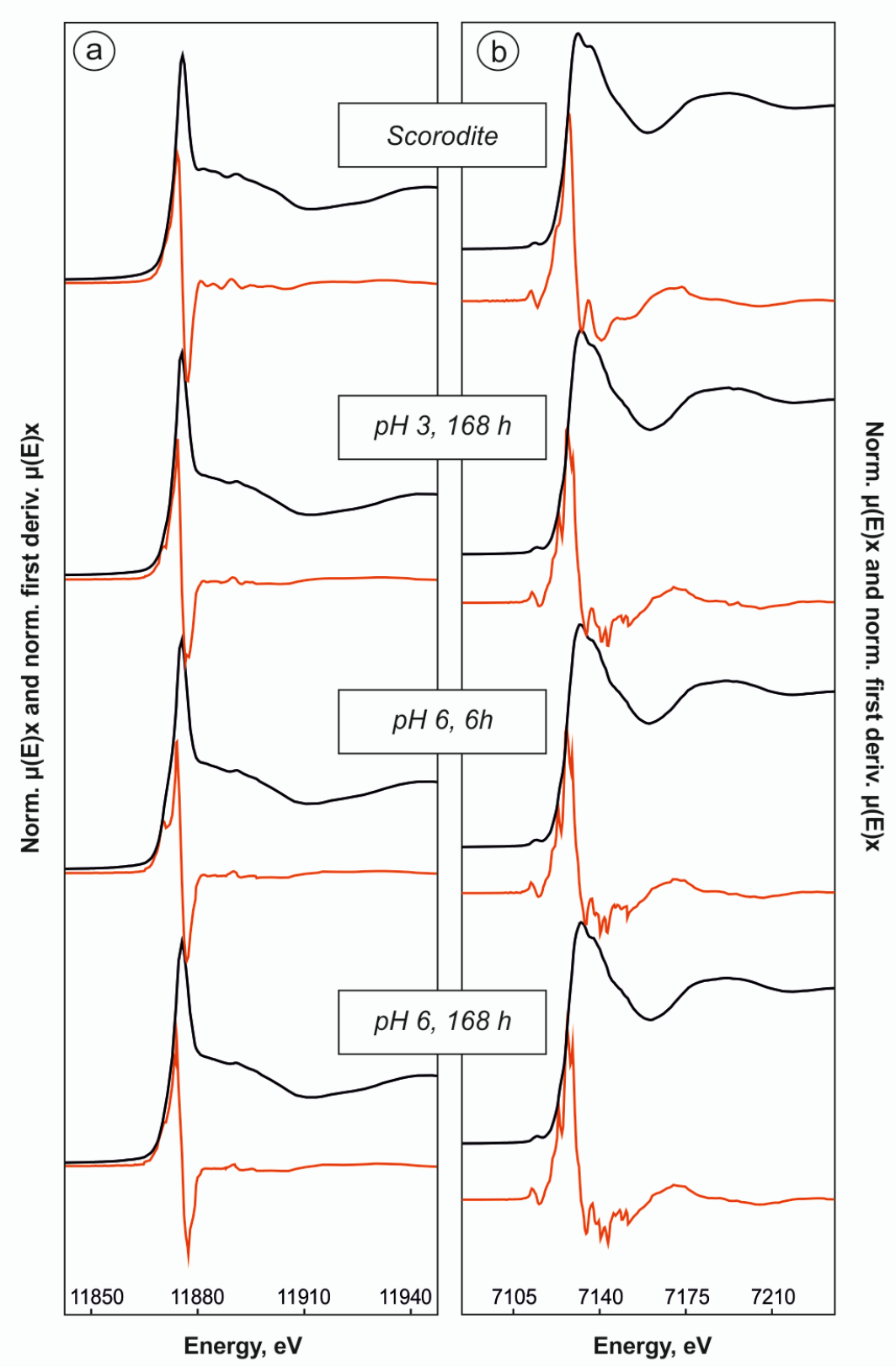

Fig S4 Normalized As (a) and Fe (b) K-edge XANES spectra (black line) and their first derivatives (red line) of reference scorodite and the colloidal fractions (1 μm -10 nm): (ii) pH 3, t=168 h; (iii) pH 6, t=6h; (iv) pH 6, t=168 h.

As and Fe K-edge EXAFS spectra were fit by linear least-squares combination fits (LCF) of reference compound spectra (k^3-weighted; 2-11 $Å^{-1}$ for Fe and 2-12.5 $Å^{-1}$ for As). First, the entire library (sixteen spectra for Fe, twelve spectra for As) was screened to determine combinations of reference spectra that best matched the data. On the basis of their occurrence and relevance in preliminary fits, the following reference spectra were included in the final EXAFS fits: An arsenate (scorodite) and As(V) sorbed onto Fe(III)-(hydr)oxides (ferrihydrite) were selected for As LCF analyses; two different Fe(III)-(hydr)oxides (e.g., scorodite, hematite) were selected for Fe LCF analyses. In the case of As, starting from the best fit with one component, the number of components *n* was increased as long as the normalized sum of the squared residuals ($NSSR = \sum(data_i - fit_i)^2/\sum(data_i)^2$) of best *n* + 1-component fit was at least 10% lower than the NSSR of the best *n*-component fit. In the Fe LCF, the best *n* + 1-component fit was considered to be significantly better than the best *n*-component fit if its NSSR was at least 20% lower and if no component accounted for less than 5% of the total Fe spectrum. Linear combination fits were not constrained to sum 100% (Table 4). More details of reference compound spectra, including their synthesis and reference publications, are shown in Table S1.

Table S1 As and Fe reference compounds used for linear combination fitting.

As standards				
Name	**Group**	**Type**	**Beamline**	**Source**
Scorodite	Arsenate	Natural	BL 4-3, SSRL	Savage et al. [5]
As(V) sorbed to ferrihydrite	Fe(III) oxide	Synthetic	BL 4-3, SSRL	Root et al. [6]
Fe standards				
Name	**Group**	**Type**	**Beamline***	**Source**
Scorodite	Oxi-arsenate	Natural	BL 4-3, SSRL	Savage et al. [5]
Hematite	Oxide	Natural	BL 4-1, SSRL	O'Day et al. [7]
Goethite	Oxide	Natural	BL 4-1, SSRL	O'Day et al. [7]

*SSRL: Stanford Synchrotron Radiation Lightsource.

Least-squares fitting of k^3-weighted Fe and As K-edge spectra were performed using the program Artemis [8]. Theoretical single- and multiple- scattering paths used to model the Fe and the As K-edge EXAFS spectra were calculated from the structure of scorodite [9] using FEFF 8.2 [10] (Tables S2 and S3).

The As K-edge EXAFS spectra were fit in *R*-space over a distance $R + \Delta R$ of 0.8 –3.6 Å (k-weigh = 3, Kaiser-Bessel window sill = 2 $Å^{-1}$). Two single-scattering (SS) paths were used to model the spectra: As-O and As-Fe. Multiple scattering (MS) within AsO_4 tetrahedra was accounted for by a three-legged triangular As–O–O MS path (degeneracy = 12). According to Mikutta et al. [4], the addition of four-legged MS paths involving As and O atoms were of minor importance to model the As K-edge EXAFS of scorodite. In addition, the low data quality of the EXAFS spectra supported the use of only the triangular As–O–O MS path. While the degeneracies of the MS path were fixed to their theoretical value, their half path lengths were expressed as a function of the SS As–O half path length assuming an ideal tetrahedron. The half path length of the triangular As–O–O MS path were set to 1.8165 ($= 1 + \sqrt{(2/3)}$) times the half path length of the As–O SS . The Debye-Waller parameters for the MS paths were constrained by considering the correlation between the lengths of individual legs [11]. Assuming that the lengths of the As–O and the O–As leg of the triangular As–O–O MS path are not correlated, their contribution to the σ^2 of MS half path length equals half the σ^2 of As–O SS path. However, because also the O–O leg contributes to the σ^2 of the MS path, we assumed the σ^2 of the MS path to be equal to the σ^2 of the As–O SS path [12]. The k^3-weighted Fe K-edge EXAFS spectra were Fourier-transformed over the k-range 2.5 – 10.5 $Å^{-1}$ using a Kaiser-Bessel window (sill width = 2.5 $Å^{-1}$). The fits were performed in *R*-space over a distance $R + \Delta R$ of 0.9 – 3.8 Å. Shell fits include two SS paths for the first and second coordination shells of Fe (Fe –O, Fe–As). In addition, one

MS within FeO_6 octahedra was accounted for: a triangular Fe–O–O MS path (degeneracy = 24, $\sigma^2 = \sigma^2$ (Fe–O SS)). The half path length of the triangular Fe–O–O MS path were set to 1.7071 (= $1 + \frac{\sqrt{2}}{2}$) times the half path length of the Fe–O SS _ENREF_17[13].

Table S2 Shell-fit results for As K-edge EXAFS spectra of selected colloidal fractions (1 µm-10 nm) from mine waste after leaching. Theoretical single- and multiple-scattering paths were calculated from the structure of scorodite [9] using FEFF 8.2 [10].

As shell-fit parameters *a*									
Sample	**Path**	**N** *b*	**R** *c* **(Å)**	**S_0^2** *d*	**σ^2** *e* **($Å^2$)**	**ΔE** *f* **(eV)**	**Fit range (Å)**	**R-factor** *g*	**red γ^2** *h*
pH 3,	*As-O*	**4**	1.70	1.05	0.0025	4.33	2.5-10.5	0.0424	2.37×10^{7}
168 h	*As-Fe*	**2**	3.36	1.05	0.0044				
	MS1 *i*	**12**	3.11	1.05	0.0100				
pH 6,	*As-O*	**4**	1.69	1.05	0.0018	4.17	2.5-10.5	0.0397	1.49×10^{7}
6 h	*As-Fe*	**2**	3.36	1.05	0.0023				
	MS1 *i*	**12**	3.08	1.05	0.0065				
pH 6,	*As-O*	**4**	1.69	1.05	0.0017	4.34	2.5-10.5	0.0472	0.76×10^{7}
168 h	*As-Fe*	**2**	3.36	1.05	0.0035				
	MS1 *i*	**12**	3.09	1.05	0.0073				

[a] According to Xu et al. [14], the crystallographic distances for scorodite are: As-O = 1.67-1.69 Å, As-Fe = 3.37-3.39 Å, As-O-O = 3.06-3.08 Å.
[b] Degeneracy (coordination number for single scattering paths), values in bold were fixed during shell fitting
[c] Half path length (inter-atomic distance for single scattering paths), uncertainty for As-O ± 0.013-0.015 Å, for As-Fe ± 0.0033-0.0037 Å, for Fe-O ± 0.013-0.016 Å
[d] Amplitude correction factor, constrained to the same value for all paths in a simultaneous fit
[e] Debye-Waller parameter, uncertainty for As-O ± 0.0010-0.0016 $Å^2$, for As-Fe ± 0.0032-0.0040 $Å^2$, for Fe-O ± 0.0017-0.0022 $Å^2$
[f] Energy shift, constrained to the same value for all paths in a simultaneous fit, uncertainty < ± 1.2 eV
[g] Normalized sum of the squared residuals of the fit ($R = \sum(data-fit)^2 / \sum data^2$)
[h] Reduced γ^2 (Stern et al. [15])

[i] *MS1 = Triangular As-O-O MS path within As(V) tetrahedron, degeneracy = 12*

Table S3 Shell-fit results for Fe K-edge EXAFS spectra of selected colloidal fractions (1 μm-10 nm) from mine waste after leaching. Theoretical single- and multiple-scattering paths were calculated from the structure of scorodite [9] using FEFF 8.2 [10].

Fe shell-fit parameters [a]									
Sample	**Path**	**N** [b]	**R** [c] **(Å)**	$\mathbf{S_0^2}$ [d]	$\boldsymbol{\sigma^2}$ [e] **(Å^2)**	**ΔE** [f] **(eV)**	**Fit range (Å)**	**R-factor** [g]	**red $\boldsymbol{\gamma^2}$** [h]
pH 3,	*Fe-O*	**6**	1.98	1.05	0.0078	- 4.05	2.5-10.5	0.0375	0.84x10^6
168 h	*Fe-As*	**4**	3.33	1.05	0.0068				
	MS2 [i]	**24**	3.44	1.05	0.0078				
pH 6,	*Fe-O*	**6**	1.98	1.05	0.0080	- 3.69	2.5-10.5	0.0283	1.52x10^6
6 h	*Fe-As*	**4**	3.34	1.05	0.0072				
	MS2 [i]	**24**	3.45	1.05	0.0081				
pH 6,	*Fe-O*	**6**	1.98	1.05	0.0080	- 4.08	2.5-10.5	0.0264	2.13x10^6
168 h	*Fe-As*	**4**	3.33	1.05	0.0071				
	MS2 [i]	**24**	3.43	1.05	0.0081				

[a] *Acording to Xu et al. [14], the crystallographic distances for scorodite are: Fe-O = 1.96-1.99 Å, Fe-As = 3.35-3.39 Å, Fe-O-O = 3.39-3.42 Å.*
[b] *Degeneracy (coordination number for single scattering paths), values in bold were fixed during shell fitting*
[c] *Half path length (inter-atomic distance for single scattering paths), uncertainty for As-O ± 0.013-0.015 Å, for As-Fe ± 0.0033-0.0037 Å, for Fe-O ± 0.013-0.016 Å*
[d] *Amplitude correction factor, constrained to the same value for all paths in a simultaneous fit*
[e] *Debye-Waller parameter, uncertainty for As-O ± 0.0010-0.0016 Å^2, for As-Fe ± 0.0032-0.0040 Å^2, for Fe-O ± 0.0017-0.0022 Å^2*
[f] *Energy shift, constrained to the same value for all paths in a simultaneous fit, uncertainty < ± 1.2 eV*
[g] *Normalized sum of the squared residuals of the fit ($R = \sum(data-fit)^2 / \sum data^2$)*
[h] *Reduced γ^2 (Stern et al. [15])*
[i] *MS2 = Triangular Fe-O-O MS path within Fe(III) octahedron, degeneracy = 24*

REFERENCES

1. Recio-Vazquez L, Garcia-Guinea J, Carral P, Maria Alvarez A, Garrido F (2011) Arsenic mining waste in the catchment area of the Madrid Detrital Aquifer (Spain). Water Air and Soil Pollution 214 (1-4):307-320.

2. Helmhart M, O'Day PA, Garcia-Guinea J, Serrano S, Garrido F (2012) Arsenic, Copper, and Zinc Leaching through Preferential Flow in Mining-Impacted Soils. Soil Science Society of America Journal 76 (2):449-462.

3. Gomez-Gonzalez MA, Serrano S, Laborda F, Garrido F (2014) Spread and partitioning of arsenic in soils from a mine waste site in Madrid province (Spain). Science of the Total Environment 500–501 (0):23-33.

4. Mikutta C, Mandaliev PN, Kretzschmar R (2013) New Clues to the Local Atomic Structure of Short-Range Ordered Ferric Arsenate from Extended X-ray Absorption Fine Structure Spectroscopy. Environmental Science & Technology 47 (7):3122-3131.

5. Savage KS, Bird DK, O'Day PA (2005) Arsenic speciation in synthetic jarosite. Chemical Geology 215 (1-4):473-498.

6. Root RA, Vlassopoulos D, Rivera NA, Rafferty MT, Andrews C, O'Day PA (2009) Speciation and natural attenuation of arsenic and iron in a tidally influenced shallow aquifer. Geochimica Et Cosmochimica Acta 73 (19):5528-5553.

7. O'Day PA, Rivera N, Root R, Carroll SA (2004) X-ray absorption spectroscopic study of Fe reference compounds for the analysis of natural sediments. American Mineralogist 89 (4):572-585

8. Ravel B, Newville M (2005) Athena and Artemis: interactive graphical data analysis using IFEFFIT. Physica Scripta T115:1007–1010

9. Kitahama K, Kiriyama R, Baba Y (1975) Refinement of crystal-structure of scorodite. Acta Crystallographica Section B-Structural Science 31 (JAN15):322-324.

10. Ankudinov AL, Rehr JJ (2000) Theory of solid-state contributions to the x-ray elastic scattering amplitude. Physical Review B 62 (4):2437-2445.

11. Hudson EA, Allen PG, Terminello LJ, Denecke MA, Reich T (1996) Polarized x-ray-absorption spectroscopy of the uranyl ion: Comparison of experiment and theory. Physical Review B 54 (1):156-165

12. Voegelin A, Weber FA, Kretzschmar R (2007) Distribution and speciation of arsenic around roots in a contaminated riparian floodplain soil: Micro-XRF element mapping and EXAFS spectroscopy. Geochimica Et Cosmochimica Acta 71 (23):5804-5820.

13. Voegelin A, Kaegi R, Frommer J, Vantelon D, Hug SJ (2010) Effect of phosphate, silicate, and Ca on Fe(III)-precipitates formed in aerated Fe(II)- and As(III)-containing water studied by X-ray absorption spectroscopy. Geochimica Et Cosmochimica Acta 74 (1):164-186.

14. Xu Y, Zhou GP, Zheng XF (2007) Redetermination of iron(III) arsenate dihydrate. Acta Crystallographica Section E: Structure Reports Online 63 (3):i67-i69.

15. Stern EA, Newville M, Ravel B, Yacoby Y, Haskel D (1995) The UWXAFS analysis package - Philosophy and details. Physica B 208 (1-4):117-120.